



Nanoscale

The Unrevealed 3D Morphological Evolution for Annealed Nanoporous Thin Films

Journal:	<i>Nanoscale</i>
Manuscript ID	NR-ART-07-2022-004014.R2
Article Type:	Paper
Date Submitted by the Author:	18-Oct-2022
Complete List of Authors:	<p>Ma, Jianqiang; Huazhong University of Science and Technology Wang, Sien; The University of Arizona, Aerospace and Mechanical Engineering Wan, Xiao; Huazhong University of Science and Technology, School of Energy and Power Engineering Ma, Dengke; Nanjing Normal University, School of Physics and Technology Xiao, Yue; The University of Arizona, Aerospace and Mechanical Engineering Hao, Qing; The University of Arizona, Aerospace & Mechanical Engineering Yang, Nuo; Huazhong University of Science and Technology, School of Energy and Power Engineering</p>

SCHOLARONE™
Manuscripts

The Unrevealed 3D Morphological Evolution for Annealed Nanoporous Thin Films

Jianqiang Ma^{1#}, Sien Wang^{2#}, Xiao Wan¹, Dengke Ma³, Yue Xiao², Qing Hao^{2*}, Nuo Yang^{1*}

1. School of Energy and Power Engineering, Huazhong University of Science and Technology, Wuhan 430074, China.

2. Department of Aerospace and Mechanical Engineering, University of Arizona, Tucson, AZ, 85721-0119, USA

3. NNU-SULI Thermal Energy Research Center (NSTER) & Center for Quantum Transport and Thermal Energy Science (CQTES), School of Physics and Technology, Nanjing Normal University, Nanjing 210023, China.

J.M. and S.W. contributed equally to this work.

* Corresponding email: qinghao@arizona.edu (Q.H.), nuo@hust.edu.cn (N.Y.)

Abstract

Nanoporous materials (sub-10 nm in diameter) have potential applications in chips, biosensors, thermoelectrics, desalination and other fields due to their large surface-to-volume ratio. The thermal annealing is a preferred technique to precisely control the ultra-fine nanopore size. Here, it is studied that the 3D morphological evolution of a membrane with periodic nanopores by thermal annealing. It is found that the evolution is determined by the combination of the membrane thickness, initial nanopore radius and periodic length of the porous pattern, rather than the previously suggested ratio between the membrane thickness and pore radius. High-temperature annealing experiments and molecular dynamics simulations are performed to confirm the rationality of the newly proposed model. Energy analysis demonstrates that surface energy minimization is the driving force of the morphological evolution. The local minimum of energy in the new model provides the possibility of thermal stability of nanoporous silicon as a thermoelectric material. This study provides guidance for the mass production of nanoporous membranes with high-temperature annealing.

Keywords: Nanoporous silicon, Morphological evolution, High-temperature annealing, Molecular dynamics simulation

1. Introduction

Nanoporous materials have significant applications in chips [1], biosensors [2], thermoelectrics [3], desalination [4], concentrating solar power system [5], micro/nano-electronics [6], and data storage [7] etc. These applications benefit from the large surface-to-volume ratio and unique transport and mechanical properties of nanoporous structures. Regarding biosensors, the charged biomolecules driven by an electric field pass through the nanopore one by one [8]. Their highly sensitive detection originates from the structure of pore, i.e., nanoscale pore sizes not too much larger than that for the detected biomolecule [9]. The diameter of a deoxyribonucleic acid (DNA) chain is about 2 nm, and the size of protein molecules ranges from a few nanometers to tens of nanometers [10, 11]. As a selective membrane used for water desalination, pores with a diameter less than 2 nm can retain salt ions while allowing rapid water transport [12]. The expansion of the pore size will result in an order of magnitude reduction in selectivity [4]. Good performance of the thermoelectric material is also determined by periodic nanopores with a small neck width between adjacent nanopores [13-15].

Various fabrication techniques have been studied by researchers to achieve nanopores with sub-10 nm diameters and nanometer precision [16-20]. Among them, a focused electron beam in a transmission electron microscope (TEM) [19] and a focused ion beam (FIB) [18] are two popular nanopore fabrication methods. Sub-10 nm or even atomic-sized pores can be fabricated across ultra-thin membranes or atomic-thick materials [21]. For mass production, traditional dry etching or wet etching is often employed for nanopore fabrication but the required dimension is hard to be achieved [22]. For these nanopore-fabrication techniques, the smallest nanopore diameter d is restricted by the film thickness t , with an aspect ratio $t/d < 3$ [23]. To achieve a high aspect ratio, heated nanoparticles as etching agents can be used [24].

Another approach to overcome this difficulty is to reduce the pore size by post-annealing, during which the membrane is softened and deformed to a lower surface free energy [25]. With its fine resolution and direct visual feedback during the process,

annealing under a TEM would reduce the pore to any size, with single-nanometer precision [19]. Direct thermal heating results in the shrinking of silicon dioxide nanopores with a similar mechanism [16]. Many pores can be processed in one step while keeping the surrounding surface composition the same [26, 27]. And high-temperature annealing is a common technique for the preparation of nanostructures, which has an important effect on the surface morphological and optical properties [28-30].

The surface tension of the softened silicon causes the morphological changing, shrinking or expansion, of nanopores. Base on experimental observation for the same silicon membrane, the small pores would shrink and eventually disappear, while the large pores expand [16, 19]. These different morphological changes are determined by the radius-thickness ratio according to a classical model considering the surface energy variation with pore-size changes. The structure will deform to a structure with a lower surface free energy, manifested as the shrinking or expansion of nanopore. Similar physics of shrinking or expansion has also been observed in gold sheets with nanopores [31] and in mercury films of micrometer-scale [32].

However, fewer works reveal the fundamental physics at the atomic scale. As an atomistic modeling method, molecular dynamics (MD) simulations can provide valuable insights into the physics of the formation and variation of nanoparticles and nanopores [33-37]. For instance, realistic silica nanopores are created for MD simulations by distinguishing nonbridging or bridging oxygens and adding the hydroxyl groups [38]. In addition, the melting of silicon nanoparticles is in good agreement with the experiment observation, such as the size dependence of melting point obtained from simulations [39, 40].

In this work, the deformation processes of nanoporous silicon membranes are investigated through both simulations and experiments. The initial parameters of the nanoporous membrane include the pore radius, membrane thickness and the periodic length of the nanopore array. The results obtained in the experiments and MD

simulations are normalized to a mathematical model to explain morphological changes. Besides, the simulated energy distribution and mean atomic potential energy prove a decrease in surface free energy under thermal annealing treatment. Furthermore, it is also investigated that the temperature dependence of nanopore deformation.

2. Results and discussion

2.1. Theoretical model of evolution

The schematic figure of a periodic nanoporous silicon membrane is shown in Fig. 1A, where r , h , and p are the nanopore radius, membrane thickness and periodic length, respectively. The simulation cell before relaxation is depicted in Fig. 1B, where silicon atoms have a diamond crystal configuration. After relaxation at elevated temperatures, the atoms at boundaries were re-organized to minimize the surface free energy.

The characteristic length of the theory is the size below which the surface tension is dominant compared with the gravity. The assumption of the proposed theoretical model is that the size of structure is smaller than the characteristic length.

When the periodic length is much larger than the pore radius, the film thickness is almost unchanged during the expanding or shrinking process. Storm et al. described the change in the free energy as [19]

$$\Delta F = \gamma \Delta A = 2\gamma (p^2 - \pi r^2 + \pi r h) \quad , \#(1a)$$

where γ is the surface tension of the viscous fluid, ΔA is the change in the total surface area. It can be written in a normalized form using $\Delta F^* = \Delta F / 2p^2\gamma$, $r^* = r/p$, $h^* = h/p$:

$$\Delta F^* = 1 - \pi r^{*2} + \pi r^* h^* \quad \#(1b)$$

The functional relationship between ΔF^* and r^* in Eq. (1b) is shown as the constant thickness model (CTM) in Fig. 1C. When h^* is a constant, it can be obtained that nanopores with r smaller (larger) than $h/2$ will shrink (expand) to reach a lower surface free energy.

Instead of isolated pores, an array of nanopores is often used in applications, such as phononic crystals [15, 33, 41-43]. Due to the narrow neck width between adjacent nanopores, the assumption in Eq. (1b) becomes invalid. The change in the local film thickness around pores, caused by the mass flow, should be further addressed. As two extreme cases, amorphous silicon and crystalline silicon have <3% divergence in the density [44], so the volume of the membrane can be approximated as a constant during high-temperature annealing. The model with a constant volume can thus be proposed as:

$$\Delta F = \gamma \Delta A = 2\gamma \left(p^2 - \pi r^2 + \pi r \frac{V}{p^2 - \pi r^2} \right), \#(2a)$$

or

$$\Delta F^* = 1 - \pi r^{*2} + \pi r^* \frac{V^*}{1 - \pi r^{*2}}, \#(2b)$$

where V is the volume of one period and the dimensionless $V^* = V/p^3$. Here h in Eq. (1a) is replaced with an averaged thickness associated with the volume, and Eq. (2b) is the normalized form of Eq. (2a). When the periodic length is much larger than the radius, Eq. (2b) can be simplified to Eq. (1b).

Based on Eq. (2b), the relationship between ΔF^* and r^* is shown as the constant volume model (CVM) in Fig. 1C, with V^* of 0.2. For both models, nanopores with r^* smaller than a critical value (r_c for the CVM and r_h for the CTM) will shrink to lower the surface free energy (ΔF^*). The contrast lies in the ΔF^* trend beyond the critical value. Here the CTM predicts continuously expanded nanopores for an initial r^* larger than r_h . In contrast, the CVM predicts a stable r_m as the local minimum of ΔF^* . For nanopores with an initial $r^* > r_m$, they should shrink to r_m eventually.

In Fig. 1D, the three-dimensional contour of ΔF^* more intuitively reflects the V^* dependence of nanopore deformations. The critical values r_c and r_m for the CVM are correlated with the V^* of the membrane. This can be obtained by the V^* -

dependent r_c and r_m in Fig. S1 in Supplementary Material I (SM I), which shows that $|r_m - r_c|$ decreases as V^* increases. It can also be seen from Fig. S1 that for $V^* > 0.27$, the local minimum r_m disappears and the ΔF^* increases monotonously with the increase of r^* . In this situation, nanopores with different initial radii will shrink and eventually disappear under the drive of the viscous force. For $V^* < 0.27$, nanopores with $r^* < r_c$ will shrink, whereas nanopores with $r_m > r^* > r_c$ will expand to r_m as the final status, as discussed earlier.

2.2. Observation of morphological evolution

Experimentally, nanoporous silicon membranes were prepared, with the film thickness as either 70 nm or 220 nm. Using a commercial silicon-on-insulator (SOI) wafer, the membranes were released from the substrate by etching away the buried oxide layer with diluted hydrofluoric acid. Nanopores, with their radii of ~ 50 nm to 120 nm, were then drilled using a FIB using Ga ions. After the nanopore drilling, the nanoporous silicon membranes were annealed at high temperatures to tune the nanopore diameter. The temperature was ramped up to the setpoint (annealing temperature) at a rate of 5 K/min to minimize the thermal stress inside the membrane and then maintained at the annealing temperature for 180 minutes. For suspended membranes, the impact of the substrate on their deformation [45] can be excluded so that the deformation was entirely driven by the minimization of the surface energy. Details are provided in SM II.

Figures 2A and 2C show the SEM images of two nanoporous membranes (NM-1 and NM-2) before the annealing. These nanopores were drilled in membranes of 220 nm/70 nm thickness using a FIB. The cross-sectional plan of a nanopore is trapezoidal, which is typical for such drilling processes [46]. Figures 2B (NM-1) and 2D (NM-2) display the corresponding SEM images after annealing at 1323/1223 K for 180 minutes, under nitrogen protection.

The controlled shrinking and expansion of nanopores in this experiment are

inconsistent with previous observations. For isolated nanopores, existing experiments always agree with the CTM, which is not the case for periodic nanopores addressed in this work. In Fig. 2A, the radius of nanopores in NM-1 (111 nm) is about half of its thickness (220 nm) and the structure should be stable based on the CTM. However, nanopores in NM-1 shrank in annealing experiments (Fig. 2B). For NM-2 (Figs. 2C and 2D), the CTM predicts expanded nanopores but stable nanoporous structures were found in experiments.

2.3. Morphological evolution in simulations

The evolution processes of nanopores were tracked in MD simulations (Fig. 3A). In simulations, the equilibrium MD method was used to predict the structural deformation [47, 48] (details in SM III). These structures are first equilibrated under the canonical ensemble (NVT) at 300 K for 0.15 ns, followed by relaxation under the microcanonical ensemble (NVE) for 0.25 ns. The Langevin heat reservoir is used to heat up the structures from 0.4 ns. The applied temperature needs to be appropriate, which should not only provide sufficient fluidity of soften pore edges but also avoid fast collapse of the structure. As shown in the inset of Fig. 3A, the applied temperature is 1500 K on the membrane with V^* of 0.21 and 1700 K on thicker membranes. More explanations are given in SM IV.

For the two structures with smaller volumes (V^* of 0.21 and 0.28), the nanopores expand with the annealing time and gradually saturate. For structures with larger volumes (V^* of 0.35 and 0.57), the nanopores shrank until disappeared, whereas the nanopores remained stable with V^* of 0.31. More detailed discussions will be given in the next section.

The mean atomic PE in evolution processes was also recorded to further explain the deformations of nanopores. Here the difference between the mean atomic PE of the silicon membrane and bulk silicon could represent the surface free energy. And amorphous silicon has a higher PE than crystalline silicon because of the destruction of

the atom distribution with the lowest energy. As shown in Fig. 3B, the change in mean atomic PE of three structures comes from the surface deformation and phase transition. The disappearance of the initial PE difference between the silicon membrane with (red line) and without (black line) nanopores indicates that the surface free energy of the nanoporous membrane decreases after the deformation because there was almost no deformation for the solid membrane.

From the PE distribution (the inset of Fig. 3B), it can be seen that the PE of surface atoms is higher than that for internal atoms after the silicon crystal melts. As shown in the inset of Fig. 3B, the color evolution from blue to red represents an increase in atomic PE. For the above two membrane structures, the visible atoms are mostly surface atoms, except for the z-direction atoms due to the periodic boundary. And for the bottom bulk structure, all atoms are internal atoms because of periodic boundaries in three directions. Surface atoms have a higher PE than internal atoms because they have weaker bond networks and fewer neighboring atoms. As the result, surface atoms with additional PE spontaneously tend to move away from pore edges under the viscous force, which reduces the surface free energy. The inset also shows that the nanopores cannot keep a perfect cylindrical shape after high-temperature annealing. Instead, a curved nanopore sidewall can be found, with its smallest diameter at the half film thickness location. This can be explained by considering local forces generated by the surface tension (More explanations are shown in Fig. S3 in SM V).

2.4. Analysis of evolution

As mentioned earlier, the evolution of nanopores was observed by both experiments and simulations. The observations in experiments (Fig. 4A) and MD simulations (Fig. 4B) were compared with the predictions by the CVM.

In experiments (Fig. 4A), for membranes with V^* of 0.33 and 0.42, nanopores shrank. It is consistent with the prediction of CVM in Fig. 1D that nanopores in membranes with $V^* > 0.27$ always tend to shrink. And for $V^* < 0.27$ (0.11 and 0.14

in Fig. 4A), nanopores with an initial radius greater than the critical radius r_c expanded to the vicinity of r_m , the local minimum of ΔF^* , instead of expanding indefinitely. It can also be concluded that the CVM is more suitable than the CTM for an array of nanopores. For V^* of 0.28, only slight expansion was observed, which can be attributed to the weak ΔF^* dependence on r^* around the initial point.

In simulations (Fig. 4B), the initial and final radii of the nanopores in different structures are obtained from the simulation results in Fig. 3A. The conclusion drawn from Fig. 4B is similar to the experimental results. The critical V^* for nanopores to remain stable is 0.31, slightly more than 0.27. As a boundary, nanopores expand for a smaller V^* and shrink for a larger V^* .

In Figs. 4A and 4B, the experimental and simulated results both agree well with the theoretical predictions. Combined with the theoretical curve in Figs. 4A and 4B, the final size of nanopore expansion in an array should be around r_m , as a critical nanopore size for the thermal stability of nanoporous membranes. The deformation rates of nanopores in Fig. 3A follow the $d\Delta F^*/dr^*$ slope in Fig. 4B when the deformation process is completely driven by the surface free energy. More discussions for the failure of the CTM can be found in SM VII.

Here, both the size of simulation cell (sub-10 nm) and the measured samples (sub-100 nm) are much smaller than the characteristic length of soft silicon ($\sim 100 \mu\text{m}$, derived in SM VIII). Therefore, both the simulations and the measured results can be used to validate the theoretical constant volume model.

2.5. Temperature effect on evolution

The temperature dependence of deformations is also investigated. As shown in Fig. 5A, the nanopores with the same initial structure under different annealing temperatures exhibit different expansion rates and final nanopore sizes. It can be seen that there is very little change in the size of nanopores at 1300 K due to limited fluidity of softened Si. At an increased annealing temperature, surface atoms are more likely to migrate under

the drive of the surface tension. At a temperature of 1500 K, the r^* increases to the lowest energy point r_m for the given porous structure. When the annealing temperature increases to 1700 K, the pore shape becomes non-circular and the connecting area between the pores disappears.

It also can be observed that the deformation rate of the structure can be largely affected by the annealing temperature. When the temperature reaches 1700 K, the expanding or shrinking rate is so fast and it is difficult to control the pore area accurately. At the same time, the membrane may be broken during the nanopore deformation process due to the large atomic kinetic energy and high stress. The sample breakage caused by a high stress at high temperatures could also be found in the experiment (shown in Fig. 5B). Nevertheless, the expanding/shrinking trend of nanopores is independent of the temperature.

To better evaluate the influence of the temperature on the deformation rate, both mean-squared displacement (MSD) [49] and radial distribution function (RDF) [50] are recorded in the simulation. MSD characterizes the diffusion behavior of all atoms over a period of time. As shown in Fig. 5C, when the annealing temperature is higher, the particles have a longer displacement distance and correspondingly a larger diffusion constant. RDF represents the degree of disorder caused by the melting of the initial crystal structure. As shown in Fig. 5D, the peak of RDF for structure with a higher annealing temperature is more gradual, which means a high degree of disorder for the lattice. It can be concluded that a higher temperature could accelerate the inward propagation speed of surface melting and amorphization [39].

For thermoelectrics, the thermoelectric figure of merit (ZT) of nanostructured Si usually monotonously increases with the temperature [51, 52]. In this case, the thermal stability of nanoporous Si can largely restrict its applications for high-temperature energy harvesting. As shown in Fig. 5A, even if the edge of nanopore is softened at 1500 K, the nanopore may still maintain a stable pore size r_m with the lowest surface energy, which can also be proved by the experimental results in Fig. 4A. Future studies

may be extended to general nanoporous thin films for the structure stability at high temperatures when other factors such as oxidation can be eliminated.

3. Conclusion

In summary, the evolutions of nanopores in silicon membranes during high-temperature annealing are systematically studied by both experiments and MD simulations. Compared with the previous assumption of a constant membrane thickness to predict the final size of the nanopore, the proposed constant volume model is proven to be more accurate for periodic nanoporous structures. The major difference is the prediction of a stable nanopore radius as the local minimum of surface free energy for some cases, which may be used to maintain nanofeatures at a high temperature.

In molecular dynamics analysis, a higher potential energy is found for surface atoms due to the dangling chemical bonds. The mass flow driven by the surface tension is to reduce the surface free energy to achieve a more stable structure. The expansion/shrinking dynamics mainly depends on the initial configuration of the nanoporous pattern. The annealing temperature has strong influence on the deformation rate of nanopores but does not affect the pore expansion/shrinking trend. In practice, an excessive annealing temperature would cause the membrane to break due to large strains in the morphological evolution process.

This work reveals the mechanism of morphology evolution of nanopores and provides guidance for the mass production of nanoporous membranes.

Conflicts of interest

There are no conflicts of interest to declare.

Acknowledgements

N.Y. is sponsored by the National Key Research and Development Project of China

No. 2018YFE0127800, and Fundamental Research Funds for the Central Universities No. 2019kfyRCPY045. Q.H. acknowledges the support from the Craig M. Berge Dean's Fellowship. FIB and TEM analyses were performed at the Kuiper Materials Imaging and Characterization facility and Q.H. gratefully acknowledges NSF (grant #1531243) for funding of the instrumentation in the Kuiper Materials Imaging and Characterization Facility at the University of Arizona. We are grateful to Shichen Deng, Ke Xu and Lina Yang for useful discussions. N.Y. thanks the National Supercomputing Center in Tianjin (NSCC-TJ) and the China Scientific Computing Grid (ScGrid) for providing assistance in computations.

References

- [1] M. Brinker, G. Dittrich, C. Richert, P. Lakner, T. Krekeler, T.F. Keller, N. Huber, P. Huber, Giant electrochemical actuation in a nanoporous silicon-polypyrrole hybrid material, *Science Advances*, 6(40) (2020) eaba1483.
- [2] K. Chen, I. Jou, N. Ermann, M. Muthukumar, U.F. Keyser, N.A.W. Bell, Dynamics of driven polymer transport through a nanopore, *Nature Physics*, (2021).
- [3] L. Yang, N. Yang, B. Li, Extreme Low Thermal Conductivity in Nanoscale 3D Si Phononic Crystal with Spherical Pores, *Nano Letters*, 14(4) (2014) 1734-1738.
- [4] S.P. Surwade, S.N. Smirnov, I.V. Vlassioux, R.R. Unocic, G.M. Veith, S. Dai, S.M. Mahurin, Water desalination using nanoporous single-layer graphene, *Nature Nanotechnology*, 10(5) (2015) 459-464.
- [5] C. Wang, W. Cheng, P. Ma, R. Xia, X. Ling, High performance Al–AlN solar spectrally selective coatings with a self-assembled nanostructure AlN anti-reflective layer, *Journal of Materials Chemistry A*, 5(6) (2017) 2852-2860.
- [6] J.-K. Hong, H.-S. Yang, M.-H. Jo, H.-H. Park, S.-Y. Choi, Preparation and characterization of porous silica xerogel film for low dielectric application, *Thin Solid Films*, 308-309 (1997) 495-500.
- [7] G. Wang, Y. Yang, J. Lee, V. Abramova, H. Fei, G. Ruan, E.L. Thomas, J.M. Tour, Nanoporous Silicon Oxide Memory, *Nano Letters*, 14(8) (2014) 4694-4699.
- [8] M. Wanunu, W. Morrison, Y. Rabin, A.Y. Grosberg, A. Meller, Electrostatic focusing of unlabelled DNA into nanoscale pores using a salt gradient, *Nature Nanotechnology*, 5(2) (2010) 160-165.
- [9] M.-H. Lee, A. Kumar, K.-B. Park, S.-Y. Cho, H.-M. Kim, M.-C. Lim, Y.-R. Kim, K.-B. Kim, A Low-Noise Solid-State Nanopore Platform Based on a Highly Insulating Substrate, *Scientific Reports*, 4(1) (2014) 7448.
- [10] A. Singer, S. Rapireddy, D.H. Ly, A. Meller, Electronic Barcoding of a Viral Gene at the Single-Molecule Level, *Nano Letters*, 12(3) (2012) 1722-1728.
- [11] L.J. Steinbock, S. Krishnan, R.D. Bulushev, S. Borgeaud, M. Blokesch, L. Feletti,

- A. Radenovic, Probing the size of proteins with glass nanopores, *Nanoscale*, 6(23) (2014) 14380-14387.
- [12] D. Cohen-Tanugi, J.C. Grossman, Water Desalination across Nanoporous Graphene, *Nano Letters*, 12(7) (2012) 3602-3608.
- [13] S. Alaie, D.F. Goettler, M. Su, Z.C. Leseman, C.M. Reinke, I. El-Kady, Thermal transport in phononic crystals and the observation of coherent phonon scattering at room temperature, *Nature Communications*, 6(1) (2015) 7228.
- [14] Y. Liao, T. Shiga, M. Kashiwagi, J. Shiomi, Akhiezer mechanism limits coherent heat conduction in phononic crystals, *Physical Review B*, 98(13) (2018) 134307.
- [15] Y. Xiao, Q. Chen, D. Ma, N. Yang, Q. Hao, Phonon Transport within Periodic Porous Structures — From Classical Phonon Size Effects to Wave Effects, *ES Materials & Manufacturing*, 5 (2019) 2-18.
- [16] W. Asghar, A. Ilyas, J.A. Billo, S.M. Iqbal, Shrinking of Solid-state Nanopores by Direct Thermal Heating, *Nanoscale Research Letters*, 6 (2011) 1-6.
- [17] C. Jian, D. Tao, L. Zewen, S. Haizhi, Controllable shrinking of silicon oxide nanopores by high temperature annealing, in: 2017 China Semiconductor Technology International Conference (CSTIC), 12-13 March 2017, IEEE, Piscataway, NJ, USA, 2017, pp. 3 pp.
- [18] J. Li, D. Stein, C. McMullan, D. Branton, M.J. Aziz, J.A. Golovchenko, Ion-beam sculpting at nanometre length scales, *Nature*, 412(6843) (2001) 166-169.
- [19] A.J. Storm, J.H. Chen, X.S. Ling, H.W. Zandbergen, C. Dekker, Fabrication of solid-state nanopores with single-nanometre precision, *Nature Materials*, 2(8) (2003) 537-540.
- [20] A.J. Storm, J.H. Chen, X.S. Ling, H.W. Zandbergen, C. Dekker, Electron-beam-induced deformations of SiO₂ nanostructures, *Journal of Applied Physics*, 98(1) (2005) 014307.
- [21] C.J. Russo, J.A. Golovchenko, Atom-by-atom nucleation and growth of graphene nanopores, *Proceedings of the National Academy of Sciences*, 109(16) (2012)

5953.

- [22] S.R. Park, H. Peng, X.S. Ling, Fabrication of Nanopores in Silicon Chips Using Feedback Chemical Etching, *Small*, 3(1) (2007) 116-119.
- [23] A.M. Marconnet, M. Asheghi, K.E. Goodson, From the Casimir Limit to Phononic Crystals: 20 Years of Phonon Transport Studies Using Silicon-on-Insulator Technology, *Journal of Heat Transfer*, 135(6) (2013) 061601.
- [24] N.R. Kadasala, M. Saei, G.J. Cheng, A. Wei, Dry Etching with Nanoparticles: Formation of High Aspect-Ratio Pores and Channels Using Magnetic Gold Nanoclusters, *Advanced Materials*, 30(3) (2018) 1703091.
- [25] Y.S. Nagornov, Thermodynamics of annealing of nanoporous silicon, *Technical Physics Letters*, 41(6) (2015) 532-536.
- [26] C.J. Lo, T. Aref, A. Bezryadin, Fabrication of symmetric sub-5 nm nanopores using focused ion and electron beams, *Nanotechnology*, 17(13) (2006) 3264-3267.
- [27] D. Tao, C. Jian, L. Mengwei, L. Zewen, Shrinking of silicon nanopore arrays by direct dry-oxygen oxidation, in: 2013 IEEE 13th International Conference on Nanotechnology (IEEE-NANO), 5-8 Aug. 2013, IEEE, Piscataway, NJ, USA, 2013, pp. 586-589.
- [28] N.A.M. Noor, S.K. Mohamad, S.S. Hamil, M. Devarajan, M.Z. Pakhuruddin, Effects of annealing temperature towards surface morphological and optical properties of black silicon fabricated by silver-assisted chemical etching, *Materials Science in Semiconductor Processing*, 91 (2019) 167-173.
- [29] A.M. Alwan, M.Q. Zayer, The Effects of Rapid Thermal Annealing on Photoluminescence Properties of Nanostructures Silicon, *Al-Nahrain Journal of Science*, 15(2) (2012) 88-92.
- [30] L. Jacobsohn*, D. Cooke, B. Bennett, R. Muenchausen, M. Nastasi, Effects of thermal annealing and ageing on porous silicon photoluminescence, *Philosophical Magazine*, 85(23) (2005) 2611-2620.
- [31] M. Lanxner, C. Bauer, R. Scholz, Evolution of hole size and shape in $\{100\}$, $\{110\}$

- and {111} monocrystalline thin films of gold, *Thin Solid Films*, 150(2-3) (1987) 323-335.
- [32] G. Taylor, D. Michael, On making holes in a sheet of fluid, *Journal of Fluid Mechanics*, 58(4) (1973) 625-639.
- [33] D. Ma, H. Ding, H. Meng, L. Feng, Y. Wu, J. Shiomi, N. Yang, Nano-cross-junction effect on phonon transport in silicon nanowire cages, *Physical Review B*, 94(16) (2016) 165434.
- [34] L. Yang, N. Yang, B. Li, Thermoelectric properties of nanoscale three dimensional Si phononic crystals, *International Journal of Heat and Mass Transfer*, 99 (2016) 102-106.
- [35] H. Wang, S. Hu, K. Takahashi, X. Zhang, H. Takamatsu, J. Chen, Experimental study of thermal rectification in suspended monolayer graphene, *Nature communications*, 8(1) (2017) 1-8.
- [36] S. Hu, Z. Zhang, P. Jiang, J. Chen, S. Volz, M. Nomura, B. Li, Randomness-induced phonon localization in graphene heat conduction, *The journal of physical chemistry letters*, 9(14) (2018) 3959-3968.
- [37] S. Hu, Z. Zhang, P. Jiang, W. Ren, C. Yu, J. Shiomi, J. Chen, Disorder limits the coherent phonon transport in two-dimensional phononic crystal structures, *Nanoscale*, 11(24) (2019) 11839-11846.
- [38] J. Geske, M. Vogel, Creating realistic silica nanopores for molecular dynamics simulations, *Molecular Simulation*, 43(1) (2016) 13-18.
- [39] K.C. Fang, C.I. Weng, An investigation into the melting of silicon nanoclusters using molecular dynamics simulations, *Nanotechnology*, 16(2) (2005) 250-256.
- [40] I.V. Talyzin, M.V. Samsonov, V.M. Samsonov, M.Y. Pushkar, V.V. Dronnikov, Size Dependence of the Melting Point of Silicon Nanoparticles: Molecular Dynamics and Thermodynamic Simulation, *Semiconductors*, 53(7) (2019) 947-953.
- [41] C. Zhou, N. Tambo, E.M. Ashley, Y. Liao, J. Shiomi, K. Takahashi, G.S.W. Craig,

- P.F. Nealey, Enhanced Reduction of Thermal Conductivity in Amorphous Silicon Nitride-Containing Phononic Crystals Fabricated Using Directed Self-Assembly of Block Copolymers, *ACS Nano*, 14(6) (2020) 6980-6989.
- [42] R. Anufriev, J. Maire, M. Nomura, Reduction of thermal conductivity by surface scattering of phonons in periodic silicon nanostructures, *Physical Review B*, 93(4) (2016) 045411.
- [43] J. Maire, R. Anufriev, R. Yanagisawa, A. Ramiere, S. Volz, M. Nomura, Heat conduction tuning by wave nature of phonons, *Science Advances*, 3(8) (2017) e1700027.
- [44] J.S. Custer, M.O. Thompson, D. Jacobson, J. Poate, S. Roorda, W. Sinke, F. Spaepen, Density of amorphous Si, *Applied Physics Letters*, 64(4) (1994) 437-439.
- [45] Q. Hao, Y. Xiao, F.J. Medina, Annealing Studies of Nanoporous Si Thin Films Fabricated by Dry Etch, *ES Materials & Manufacturing*, 6 (2019) 24-27.
- [46] Q. Hao, D. Xu, H. Zhao, Y. Xiao, F.J. Medina, Thermal studies of nanoporous Si films with pitches on the order of 100 nm—Comparison between different pore-drilling techniques, *Scientific Reports*, 8(1) (2018) 1-9.
- [47] L. de Sousa Oliveira, N. Neophytou, Large-scale molecular dynamics investigation of geometrical features in nanoporous Si, *Physical Review B*, 100(3) (2019).
- [48] A.J. McGaughey, M. Kaviani, Phonon transport in molecular dynamics simulations: formulation and thermal conductivity prediction, *Advances in Heat Transfer*, 39 (2006) 169-255.
- [49] J.-P. Hansen, I.R. McDonald, *Theory of simple liquids*, Elsevier, 1990.
- [50] J.G. Kirkwood, E.M. Boggs, The radial distribution function in liquids, *The Journal of Chemical Physics*, 10(6) (1942) 394-402.
- [51] Q. Hao, D. Xu, N. Lu, H. Zhao, High-throughput Z T predictions of nanoporous bulk materials as next-generation thermoelectric materials: A material genome approach, *Physical Review B*, 93(20) (2016) 205206.
- [52] Q. Hao, G. Zhu, G. Joshi, X. Wang, A. Minnich, Z. Ren, G. Chen, Theoretical

studies on the thermoelectric figure of merit of nanograined bulk silicon, *Applied Physics Letters*, 97(6) (2010) 063109.

Fig. 1 (A) Schematic of nanoporous silicon membrane. (B) Schematic views of simulation cell of crystalline silicon structure with round pores. The red atoms represent the surface atoms located on the sidewall of the nanopore. (C) The change of surface free energy (ΔF^*) with the normalized radius (r^*) for the CVM, in comparison to the CTM. The dimensionless parameters are: $\Delta F^* = \Delta F/(2p^2\gamma)$, $V^* = V/p^3$, $h^* = h/p$, $r^* = r/p$. It can be seen that for the CVM, the surface free energy reaches the peak at r_c and reaches the trough at r_m , while for CTM, the curve only has maximum r_h . (D) Comparison of the volume dependences obtained from the CVM. The color change from red to purple means that ΔF^* is decreasing, and parallel gray curves represent V^* as different constants.

Fig. 2 SEM images (top view) of two nanoporous membranes, NM-1 and NM-2. NM-1: (A) before and (B) after the high-temperature annealing. NM-2: (C) before and (D) after the high-temperature annealing. For NM-1 (NM-2), the pitch p is 400 nm (200 nm), nanopore radius r is 111 nm (52 nm), and film thickness h is 220 nm (70 nm).

Fig. 3 (A) The size evolution of nanopores based on different V^* values in the simulation. The temperature evolutions of several structures are illustrated in the inset. (B) Mean atomic PE evolution with time. In comparison, the black curve represents a solid membrane whose thickness is the same as that for a nanoporous membrane with $V^*=0.21$. The blue curve represents bulk silicon. The inset is the PE distribution of the three configurations.

Fig. 4 The normalized surface free energy (ΔF^*) versus the normalized radius (r^*). (A) Comparison between experimental and theoretical results. The solid symbols represent the initial structure, and the hollow symbols represent the evolved structure after the high-temperature annealing. Curves for different V^* values in the CVM are plotted. (B) Comparison between simulation and theoretical results. Again, solid and hollow symbols represent the nanopore sizes before and after high-temperature annealing, respectively. The lines are theoretical calculations based on Eq. (2b) and the solid symbols are measurements (Fig. 4A) or simulations (Fig. 4B). The original data are shown in Table S2 in SM VI.

Fig. 5 (A) Nanopore evolution at different temperatures, with V^* fixed at 0.21. The temperature evolutions are illustrated in the inset in Fig. 5C. (B) SEM image of a damaged nanoporous membrane treated at 1323 K. (C) Mean-squared displacement of all atoms at different temperatures. (D) Radial distribution functions of annealed nanoporous membranes at 0.05 ns. Curves of different colors represent the state of the same nanoporous membrane at different annealing temperatures.

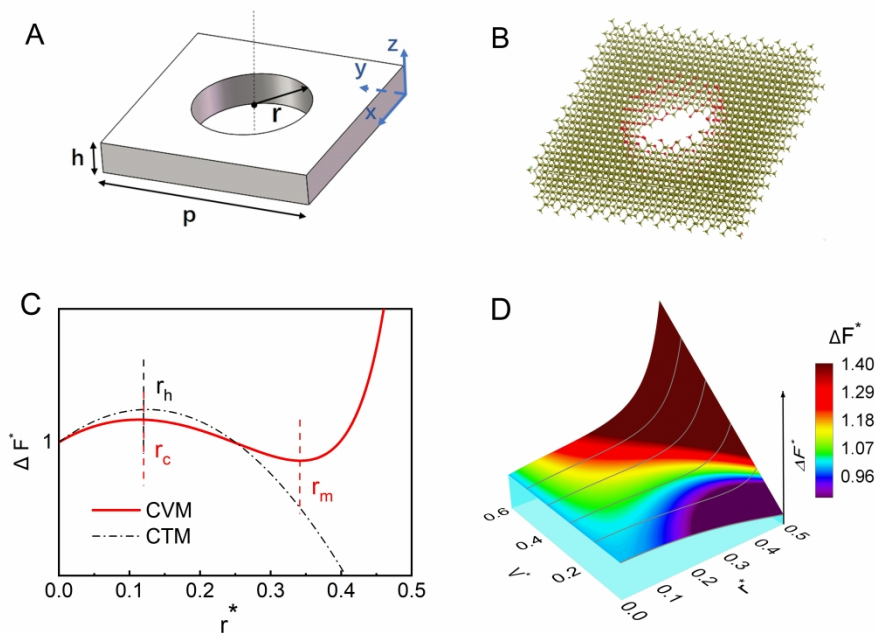


Fig. 1 (A) Schematic of nanoporous silicon membrane. (B) Schematic views of simulation cell of crystalline silicon structure with round pores. The red atoms represent the surface atoms located on the sidewall of the nanopore. (C) The change of surface free energy (ΔF^*) with the normalized radius (r^*) for the CVM, in comparison to the CTM. The dimensionless parameters are: $\Delta F^* = \Delta F / (2p^2 \gamma)$, $V^* = V / p^3$, $h^* = h / p$, $r^* = r / p$. It can be seen that for the CVM, the surface free energy reaches the peak at r_c and reaches the trough at r_m , while for CTM, the curve only has maximum r_h . (D) Comparison of the volume dependences obtained from the CVM. The color change from red to purple means that ΔF^* is decreasing, and parallel gray curves represent V^* as different constants.

584x406mm (300 x 300 DPI)

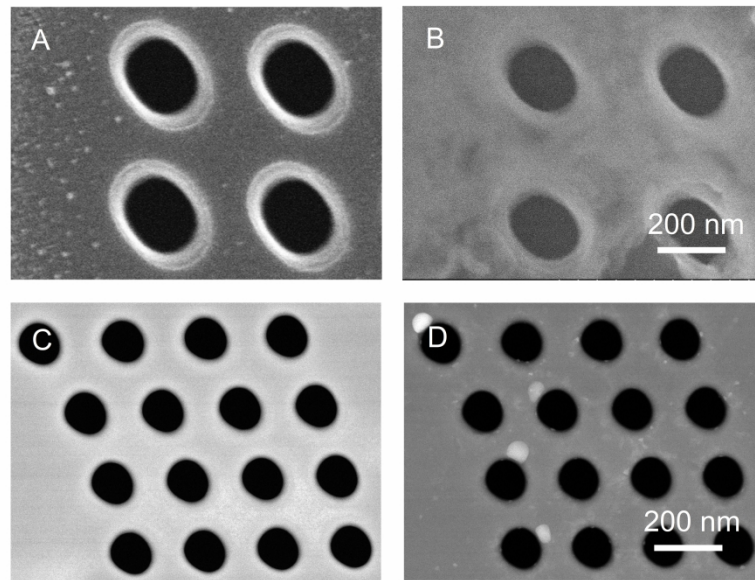


Fig. 2 SEM images (top view) of two nanoporous membranes, NM-1 and NM-2. NM-1: (A) before and (B) after the high-temperature annealing. NM-2: (C) before and (D) after the high-temperature annealing. For NM-1 (NM-2), the pitch p is 400 nm (200 nm), nanopore radius r is 111 nm (52 nm), and film thickness h is 220 nm (70 nm).

584x406mm (300 x 300 DPI)

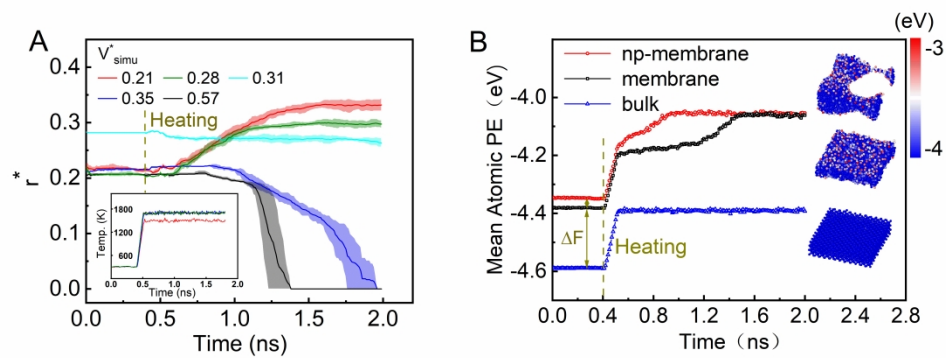


Fig. 3 (A) The size evolution of nanopores based on different V^* values in the simulation. The temperature evolutions of several structures are illustrated in the inset. (B) Mean atomic PE evolution with time. In comparison, the black curve represents a solid membrane whose thickness is the same as that for a nanoporous membrane with $V^*=0.21$. The blue curve represents bulk silicon. The inset is the PE distribution of the three configurations.

584x254mm (300 x 300 DPI)

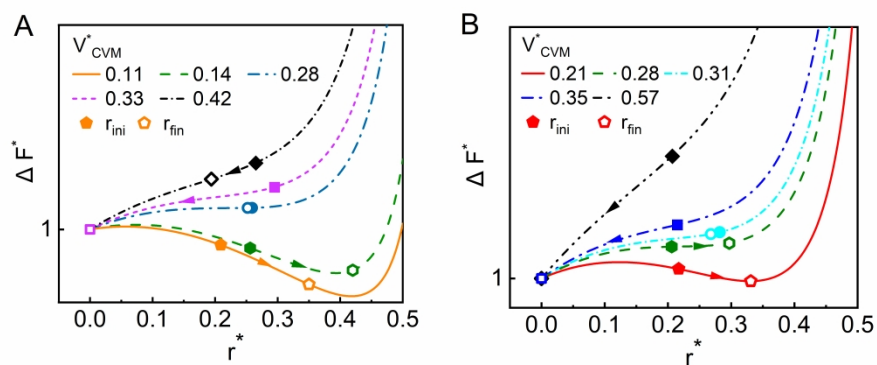


Fig. 4 The normalized surface free energy (ΔF^*) versus the normalized radius (r^*). (A) Comparison between experimental and theoretical results. The solid symbols represent the initial structure, and the hollow symbols represent the evolved structure after the high-temperature annealing. Curves for different V^* values in the CVM are plotted. (B) Comparison between simulation and theoretical results. Again, solid and hollow symbols represent the nanopore sizes before and after high-temperature annealing, respectively. The lines are theoretical calculations based on Eq. (2b) and the solid symbols are measurements (Fig. 4A) or simulations (Fig. 4B). The original data are shown in Table S2 in SM VI.

584x254mm (300 x 300 DPI)

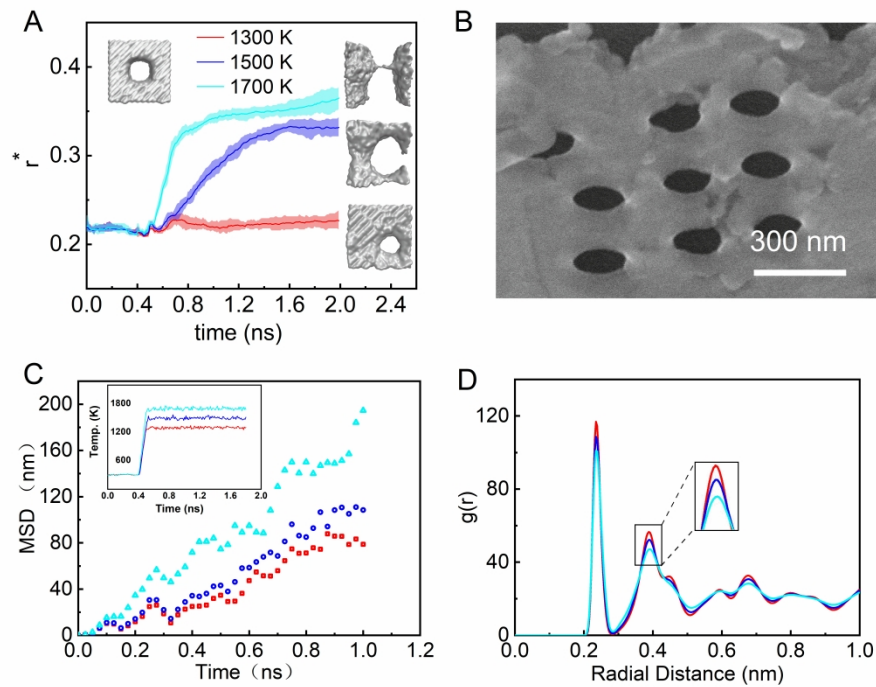


Fig. 5 (A) Nanopore evolution at different temperatures, with V^* fixed at 0.21. The temperature evolutions are illustrated in the inset in Fig. 5C. (B) SEM image of a damaged nanoporous membrane treated at 1323 K. (C) Mean-squared displacement of all atoms at different temperatures. (D) Radial distribution functions of annealed nanoporous membranes at 0.05 ns. Curves of different colors represent the state of the same nanoporous membrane at different annealing temperatures.

584x406mm (300 x 300 DPI)